Lesson 21 part 3
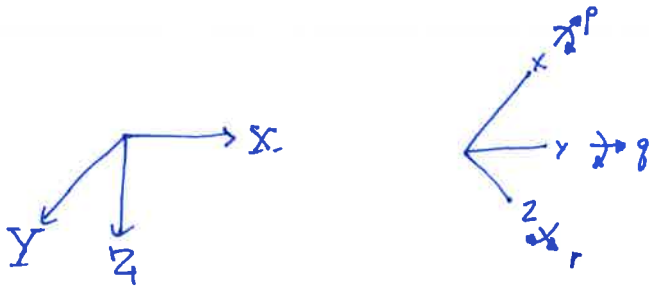
Angular velocities and Euler Angles

Angular Velocities in the body frame and Inertial Frame

How can the body frame rates be transformed to Euler Angle rates

$$\underbrace{p, q, r}$$
$$\dot{\phi}, \dot{\theta}, \dot{\psi}$$

$$
\begin{pmatrix} p \\ q \\ r \end{pmatrix} =
\begin{bmatrix}
1 & 0 & -S_\theta \\
0 & C_\phi & C_\theta S_\phi \\
0 & -S_\phi & C_\theta C_\phi
\end{bmatrix}
\begin{pmatrix} \dot{\phi} \\ \dot{\theta} \\ \dot{\psi} \end{pmatrix}
$$

For more info, see problem 5.6 in "Applied Mathematics in Integrated Navigation Systems" Rogers.

The inverse gives the Euler rates in terms of body frame rates

$$
\begin{pmatrix} \dot{\phi} \\ \dot{\theta} \\ \dot{\psi} \end{pmatrix} =
\begin{bmatrix}
1 & S_\phi \tan\theta & C_\phi T_\theta \\
0 & C_\phi & -S_\phi \\
0 & S_\phi \sec\theta & C_\phi \sec\theta
\end{bmatrix}
\begin{pmatrix} p \\ q \\ r \end{pmatrix}
$$

This allows us to take current body frame rates and EAs and advance in time the EAs.

Combined 6-DOF Aircraft Dynamics

Location:

$$\begin{pmatrix} \frac{dx}{dt} \\ \frac{dy}{dt} \\ \frac{dz}{dt} \end{pmatrix} = [B] \begin{pmatrix} u \\ v \\ w \end{pmatrix} \qquad \text{where} \quad B = f(\phi, \theta, \psi)$$

$$= \begin{bmatrix} c_\theta c_\psi & -c_\phi s_\psi + s_\phi s_\theta c_\psi & s_\phi s_\psi + c_\phi s_\theta c_\psi \\ c_\theta s_\psi & c_\phi c_\psi + s_\phi s_\theta s_\psi & -s_\phi c_\psi + c_\phi s_\theta s_\psi \\ -s_\theta & s_\phi c_\theta & c_\phi c_\theta \end{bmatrix}$$

Inertial frame / local body frame

Velocity

$$\begin{pmatrix} \dot{u} \\ \dot{v} \\ \dot{w} \end{pmatrix} = \begin{pmatrix} X/m - gw + rv \\ Y/m + ru + pw \\ Z/m - pv - qu \end{pmatrix} = \underbrace{\begin{bmatrix} 0 & r & -g \\ -r & 0 & p \\ g & -p & 0 \end{bmatrix}}_{-\Omega_B} \begin{pmatrix} u \\ v \\ w \end{pmatrix} + \underbrace{\frac{1}{m} \begin{pmatrix} X \\ Y \\ Z \end{pmatrix}}_{F_B}$$

Euler Angles / Orientation:

$$\begin{pmatrix} \dot{\phi} \\ \dot{\theta} \\ \dot{\psi} \end{pmatrix} = \underbrace{\begin{bmatrix} 1 & s_\phi \tan\theta & c_\phi \tan\theta \\ 0 & c_\phi & -s_\phi \\ 0 & s_\phi \sec\theta & c_\phi \sec\theta \end{bmatrix}}_{\Omega_E} \begin{pmatrix} p \\ q \\ r \end{pmatrix}$$

Angular Velocities

$$\begin{pmatrix} \dot{p} \\ \dot{q} \\ \dot{r} \end{pmatrix} = \begin{bmatrix} \text{Inertia} \\ \text{Matrix} \end{bmatrix}^{-1} \left[\underbrace{\begin{pmatrix} L \\ M \\ N \end{pmatrix}}_{T_B} + \overbrace{\begin{pmatrix} + qp I_{xz} \mp rp I_{xy} - (r^2 - q^2) I_{yz} - qr I_z + rq I_y \\ -rp I_x + rq I_{xy} + (r^2 - p^2) I_{xz} - pq I_{yz} + pqr I_z \\ + (p^2 - q^2) I_{xy} - pq I_y + pr I_{yz} + qp I_x - qr I_{xz} \end{pmatrix}}^{-I^{-1}\Omega_B I} \right]$$

Integration

$$y(t + \Delta t) - y(t) = \int_t^{t + \Delta t} \dot{y} \, dt$$

The 6 DOF has 12 states

$$S = \begin{bmatrix} X & Y & Z & u & v & w & p & q & r & \phi & \theta & \psi \end{bmatrix}^T = \begin{bmatrix} X \\ Y \\ Z \\ u \\ v \\ w \\ p \\ q \\ r \\ \phi \\ \theta \\ \psi \end{bmatrix}$$

$$\dot{S} = \frac{dS}{dt}$$

$$\dot{S} = \begin{bmatrix} 0 & B & 0 & 0 \\ 0 & -\Omega_B & 0 & 0 \\ 0 & 0 & -I^{-1}\Omega_B I & 0 \\ 0 & 0 & 0 & \Omega_E \end{bmatrix} \begin{pmatrix} S \end{pmatrix} + \begin{pmatrix} 0 \\ m^{-1} F_B \\ I^{-1} T_B \\ 0 \end{pmatrix}$$

- Given an initial condition S_o and F_B and T_B, the entire flight profile can be integrated forward in time.

- Given an initial condition S_o and a desired ending condition S_F, we can use F_B and T_B to controll the aircraft to the desired S_F.

- This is a non-linear differential equation,

- This formulation <u>FAILS</u> when $\theta = 90°$. why?

  - pick a pure body frame pitch up. ~~gives~~ q = constant $p = r = 0$

  $$\dot{\theta} = 0 \cdot p + \cos\overset{1}{\phi} q - \sin\overset{0}{\phi} r = q \quad (\text{looks ok, right?})$$

  $$\dot{\phi} = p + \sin\overset{0}{\phi} \tan\overset{\infty}{\theta} q + \cos\overset{1}{\phi} \tan\overset{\infty}{\theta} r = p + \infty r \;!!!$$

  $$\dot{\psi} = 0 \cdot p + \sin\overset{0}{\phi} \sec\overset{\infty}{\theta} q + \cos\overset{1}{\phi} \sec\overset{\infty}{\theta} r = \infty r \;!!$$

  <u>Gimbal lock</u> !

  Use Quaternions if θ is near $\pm 90°$ Apollo 13 antenna + FCS gimbal

Aircraft Flight Dynamics with a Non-Inertial CFD Code

Charles R. O'Neill[*] and Andrew S. Arena, Jr.[†]

Oklahoma State University

Stillwater, Oklahoma 74078

There a few typos in here!

Aircraft flight dynamics are investigated with a non-inertial, finite element, Eulerian CFD code. This project developed a fully 6 DOF rigid body dynamics solver for a non-inertial finite-element inviscid CFD solver. A non-inertial CFD formulation appears to have significant advantages for arbitrary rigid body simulations. Missile, aircraft and wedge dynamics are simulated for small and large rigid body motions. The non-inertial formulation also offered an intuitive and simple stability derivative extraction routine.

I.   Introduction

Modern flight testing involves characterizing complex, high performance flight vehicles operating over wide flight conditions and variable vehicle geometries. Simulating these coupled structural, aerodynamic, and control systems computationally allows for powerful, timely, and efficient flight test support. The Structural Analysis Routines[1] (STARS) code developed at NASA Dryden supports Dryden's flight tests with a suite of multidisciplinary tools for structural, aerodynamic, thermal, and control system analysis. STARS has powerful aeroelastic and aeroservoelastic simulation capabilities. Stability and control, and sensor simulations are also available. Recent programs supported by the STARS code include the X-29, X-33, F-18, and HyperX.[1,2]

The computational fluid dynamics (CFD) component of STARS solves the Euler and Navier-Stokes governing equations. STARS's aerodynamic solvers are not limited by governing equations but by system coupling. The recent addition of a non-inertial reference frame CFD formulation extends the capabilities of STARS to include rotational and translational motions.[3] Coupling rigid body dynamics with the non-inertial CFD opens significant possibilities for flight test support. Figure 1 conceptually shows some of these possibilities. Rigid body dynamics are needed to simulate these complex, but common, flight configurations.
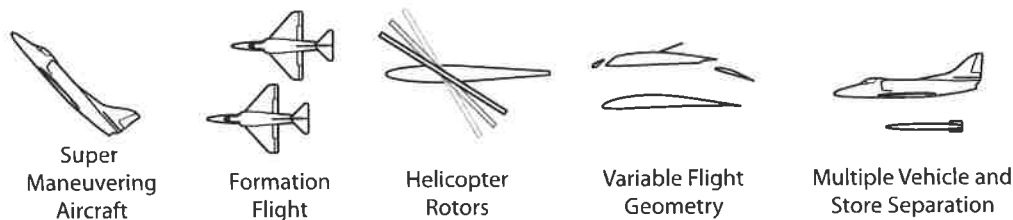

| Super Maneuvering Aircraft | Formation Flight | Helicopter Rotors | Variable Flight Geometry | Multiple Vehicle and Store Separation |

Figure 1. Rigid Body Dynamics Applications

A.   Objective

This paper's objective is to develop a 6 degree of freedom rigid body solver and then couple the rigid body solver into a computational fluid dynamics (CFD) solver. Coupling into a CFD solver requires determining

---

[*]Graduate Research Assistant, Student Member AIAA

[†]Professor, Senior Member AIAA

boundary conditions from the previous aerodynamically and inertially generated forces. This paper concentrates on the flight dynamics applications of the rigid body dynamics in an inviscid but compressible flow.

Rigid body dynamics are governed by two sets of equations: attitude representation, and body-frame motion. Attitude representation uses an inertial fixed reference frame for translations and directions. The body-frame kinematics uses translational and rotational forms of Newton's classical law.

II. Literature Review

Simulating aerospace vehicle dynamics is common. Nelson[1] derives a traditional approach to applying rigid body dynamics to aircraft. Phillips[5] reviews Euler angles, direction cosines, and quaternions for aircraft motion specification. Phillips suggests using quaternions to avoid the computational expenses and singularities inherent in the Euler angle representation. Stevens and Lewis[6] derive a quaternion approach to rigid body dynamics. Visually, Kato[7] discusses large amplitude maneuvers and their effect on motion descriptions. Store separations with multiple body dynamic simulations is a related and active field.[8–10] Recently, Rizk[11] implemented a 6 degree-of-freedom store separation dynamics simulation.

Primary references for this paper are: Aircraft Control and Simulation,[6] Flight Stability and Automatic Control,[4] and Finite Element CFD Analysis of Super-Maneuvering and Spinning Structures.[3] Babcock's paper[12] provides the stability derivative extraction methodology.

III. Attitude Representation

Attitude representation involves specifying the aircraft's position and orientation, and converting between inertial and non-inertial frames. For the scope of this paper, the inertial frame is Earth fixed, and the non-inertial frame is aircraft body-fixed.

A. Inertial and Non-Inertial Frames

The crux of attitude representation is converting between body fixed and inertial reference frames. Figure 2 shows a two-dimensional representation of an inertial frame (X,Y) and a non-inertial frame (x,y) connected by vector R. A point at vector r_b in the non-inertial frame transforms to a vector q_i in the inertial frame. The relationship is given below:

$$q_i = R_i + Br_b$$

B is a transformation operator between the body b and inertial i frames. So, B^{-1} transforms from the inertial frame to the body frame. Intuition suggests that B and B^{-1} must be similar. In fact, transformation matrices have a special property that $BB^T = I$, which implies $B^{-1} = B^T$.
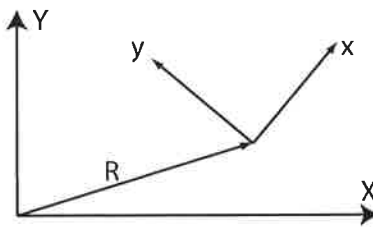

Figure 2. Coordinate Systems

B. Orientation

Orientation concerns the directionality of the body-fixed frame with respect to an inertial frame. For the scope of this project, the Earth is a sufficient inertial frame. This paper uses quaternions for orientation. The objective is to convert body frame rotations to inertial frame attitudes.

Euler angles were rejected for the well-known pitch singularity. Preliminary testing also showed that while the Euler angle singularity is at $\theta = \pm 90°$, attitude errors become noticeable earlier. For a generic motion simulations, Euler angles are unwelcome.

Quaternions have no such singularity —at the expense of an extra parameter. The quaternion form consists of four parameters: a scalar (q_0), and a vector (q_1, q_2, q_3). An extra constraint is required, $q_0^2 + q_1^2 + q_2^2 + q_3^2 = 1$. For a quaternion based representation system, the transformation matrix B is:[6]

$$B = \begin{bmatrix} q_0^2 + q_1^2 - q_2^2 - q_3^2 & 2(q_1 q_2 - q_0 q_3) & 2(q_1 q_3 + q_0 q_2) \\ 2(q_1 q_2 + q_0 q_3) & q_0^2 - q_1^2 + q_2^2 - q_3^2 & 2(q_2 q_3 - q_0 q_1) \\ 2(q_1 q_3 - q_0 q_2) & 2(q_2 q_3 + q_0 q_1) & q_0^2 - q_1^2 - q_2^2 + q_3^2 \end{bmatrix}$$

Quaternion updates are via four 1st order differential equation. The *almost-linear* quaternion differential equation is:[6]

$$\begin{bmatrix} \dot{q}_0 \\ \dot{q}_1 \\ \dot{q}_2 \\ \dot{q}_3 \end{bmatrix} = -\frac{1}{2} \begin{bmatrix} 0 & p & q & r \\ -p & 0 & -r & q \\ -q & r & 0 & -p \\ -r & -q & p & 0 \end{bmatrix} \begin{bmatrix} q_0 \\ q_1 \\ q_2 \\ q_3 \end{bmatrix}$$

Solely for human visualization, traditional Euler angles are needed. The quaternion to Euler angle conversion is:[6]

$$\begin{bmatrix} \phi \\ \theta \\ \psi \end{bmatrix} = \begin{bmatrix} \arctan\left(2(q_0 q_1 + q_2 q_3)/\left(q_0^2 - q_1^2 - q_2^2 + q_3^2\right)\right) \\ \arcsin\left(2(q_0 q_2 - q_1 q_3)\right) \\ \arctan\left(2(q_0 q_3 + q_1 q_2)/\left(q_0^2 + q_1^2 - q_2^2 - q_3^2\right)\right) \end{bmatrix} \quad \text{with the ranges} \quad \begin{matrix} -\pi \le \phi \le \pi \\ -\pi/2 \le \theta \le \pi/2 \\ -\pi \le \psi \le \pi \end{matrix}$$

Inspection of the Quaternion to Euler angle conversion shows that unity magnitude quaternions are needed to remain in the real valued arcsin() and arctan() domains. Re-normalizing the quaternion appears necessary before converting to Euler angles.

C.   Position

Inertial frame positions are calculated from body frame velocities and inertial orientation. Position updates use the B transformation matrix developed above. The translational equation is:

$$\begin{bmatrix} \dot{x} \\ \dot{y} \\ \dot{z} \end{bmatrix} = B \begin{bmatrix} u \\ v \\ w \end{bmatrix}$$

The result is three 1st order differential equations for inertial position. Integration is simple when no rotations occur.

IV.   Body Frame Kinematics

Aircraft velocity kinematics are calculated in the non-inertial (body) frame. Nelson[4] derives a set of aircraft equations of motion. Inertias are referenced to the body fixed frame. Except for certain body forces such as gravity, the body fixed equations of motion are independent of attitude.

A.   Translation

For the translational rigid body modes, the equations of motion are:[4]

$$X - mgS_\theta = m(\dot{u} + qw - rv)$$
$$Y + mgC_\theta S_\phi = m(\dot{v} + ru - pw)$$
$$Z + mgC_\theta C_\phi = m(\dot{w} + pv - qu)$$

The translation equations become nonlinear when the rotation axis is not along the translation velocity axis. Solving for the translational derivative terms yields:

$$\begin{bmatrix} \dot{u} \\ \dot{v} \\ \dot{w} \end{bmatrix} = \begin{bmatrix} 0 & r & -q \\ -r & 0 & p \\ q & -p & 0 \end{bmatrix} \begin{bmatrix} u \\ v \\ w \end{bmatrix} + \frac{1}{m} \begin{bmatrix} X - mgS_\theta \\ Y + mgC_\theta S_\phi \\ Y + mgC_\theta C_\phi \end{bmatrix}$$

The translational equation of motion consists of three 1st order nonlinear differential equations.

B.   Rotation

The rotational equations of motion in the body frame for typical symmetrical aircraft are:[4]

$$L = I_x \dot{p} - I_{xz}\dot{r} + (I_z - I_y)qr - I_{xy}pq$$
$$M = I_y \dot{q} + (I_x - I_z)rp + I_{xz}(p^2 - r^2)$$
$$N = -I_{xz}\dot{p} + I_z\dot{r} + (I_y - I_x)pq + I_{xz}qr$$

The equations are nonlinear when certain translations and rotations occur. In contrast to the single translational mass, 6 rotational inertias are possible. Solving for the rotational equations or motion for the rotational derivatives yields:

$$\begin{bmatrix} \dot{p} \\ \dot{q} \\ \dot{r} \end{bmatrix} = I^{-1} \begin{bmatrix} L - (I_z - I_y)qr + I_{xz}pq \\ M - (I_x - I_z)rp - I_{xz}(p^2 - r^2) \\ N - (I_y - I_x)pq - I_{xz}qr \end{bmatrix}$$

A general inverse inertia matrix[a] is:

$$I^{-1} = \frac{1}{\Gamma} \begin{bmatrix} I_z & 0 & I_{xz} \\ 0 & \Gamma/I_y & 0 \\ I_{xz} & 0 & I_x \end{bmatrix}$$

with

$$\Gamma = I_x I_z - I_{xz}^2$$

The rotational equation of motion consists of three 1st order nonlinear differential equations.

V.   Coupled Rigid Body Equations of Motion

The objective of this section is to show the total 6 degree of freedom rigid body dynamics equations of motion. The state vector is: $S = [x\ y\ z\ u\ v\ w\ p\ q\ r\ q_0\ q_1\ q_2\ q_3]^T$. Combining the above orientation and kinematic equations yields thirteen 1st order nonlinear differential equations. From Stevens and Lewis[6] the complete system with lumped coupling terms (Ω_B, Ω_q, I) is:

$$\dot{S} = \begin{bmatrix} 0 & B & 0 & 0 \\ 0 & -\Omega_B & 0 & 0 \\ 0 & 0 & -I^{-1}\Omega_B I & 0 \\ 0 & 0 & 0 & -\frac{1}{2}\Omega_q \end{bmatrix} S + \begin{pmatrix} 0 \\ m^{-1}F_B \\ J^{-1}T_B \\ 0 \end{pmatrix}$$

On first inspection, the system appears linear, but this is not the case since the state variable is contained inside the gradient matrix.

A.   Numerical Methods

Appropriate numerical methods are required for the quaternion governing equation —the quaternion magnitude must remain unity. Phillips[5] discusses this topic and suggests at least a 4th order ODE numerical solution. This paper uses a 4th order Adams Moulton finite difference ODE numerical integration method. The update is discrete in time based on continuous derivatives $(\dot{y})$ at four discrete timesteps.

$$y(t+1) = y(t) + \frac{dt}{24}\left(55\dot{y}(t) - 59\dot{y}(t-1) + 37\dot{y}(t-2) - 9\dot{y}(t-3)\right)$$

---

[a]This inertia matrix assumes that the only asymmetrical component is I_{xz}.

VI. Non-inertial CFD Formulation

The non-inertial CFD program (euler3d) used for this paper is developed in Cowan's Ph.D dissertation.[3] The CFD solver was developed using Euler Angles for attitude representation. The appropriate attitude terms need to be reviewed and converted to the quaternion format. This section reviews Cowan's work to describe how boundary conditions are specified. The inviscid, compressible Euler fluid dynamics governing partial differential equation in a non-inertial frame is:

$$\frac{\partial U}{\partial t} + \frac{\partial F_i}{\partial x_i} = S$$

with the following vectors

$$U = \begin{pmatrix} \rho \\ \rho u_1 \\ \rho u_2 \\ \rho u_3 \\ \rho e_r \end{pmatrix} \quad F = \begin{pmatrix} \rho u_i \\ \rho u_i u_1 \\ \rho u_i u_2 \\ \rho u_i u_3 \\ \rho u_i e_r \end{pmatrix} + \begin{pmatrix} 0 \\ p\delta_{1i} \\ p\delta_{2i} \\ p\delta_{3i} \\ p u_i \end{pmatrix} \quad S = -\rho \begin{pmatrix} 0 \\ a_t' + \Omega V_r \\ a_t' \cdot (V_t' + V_r) \end{pmatrix}$$

The source term S contains the non-inertial parts with the following source terms:

$$V_t = B^{-1}V_0 + \Omega r_b, \qquad a_t' = B^{-1}a_0 + \Omega^2 r_b + \dot{\Omega} r_b + \Omega V_r$$

$$\Omega_B = \begin{pmatrix} 0 & -\omega_z & \omega_y \\ \omega_z & 0 & -\omega_x \\ -\omega_y & \omega_x & 0 \end{pmatrix}$$

Notice, as expected, that the CFD solver uses only non-inertial (body) frame motions and the B transformation matrix. A significant advantage of this non-inertial formulation is that the CFD solver needs only a single, fixed computational grid for any arbitrary rigid body motion.

VII. Verification

The objective of this section is to establish that the rigid body equations of motion are being solved correctly.

A. Energy Conservation

This case tests for rigid body dynamics energy conservation. The concept is to give an initial motion and track the total energy. Constant energy verifies that the rigid body dynamics solver is solving the correct equations. Additionally, this testcase shows timestep sensitivities with regard to the rigid body dynamics solver.

The governing energy equation for translations and rotations is:

$$E(t) = \sum_{i=x,y,z} \frac{1}{2}m_i v_i(t)^2 + \sum_{i=p,q,r} \frac{1}{2}I_i \omega_i(t)^2$$

For this particular testcase, the masses and inertias are:

$$M = 1, \quad I_x = 1, \quad I_y = 2, \quad I_z = 3$$

For an initial body-fixed translation vector of (1,2,3) and a rotation vector of $(4\pi, 2\pi, \pi)$ radians per second, the theoretical kinetic energy is 140. A time history plot (Fig. 3) shows the non-linear behavior. Figure 4 shows the kinetic energy content for timesteps varying from 0.01 to 0.0001 —equivalent to 50 to 5000 points per highest frequency (roll rate of 720 degrees per second). Above 100 points per cycle seems appropriate; fewer points per cycle tend to artificially dampen the dynamics solution. Timestep sizes for accurate dynamics responses appear to be larger than the corresponding CFD timestep sizes.
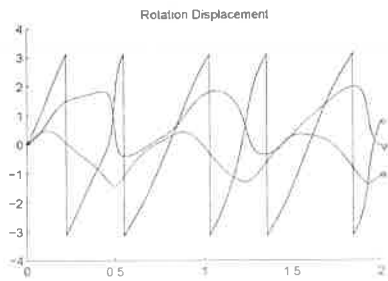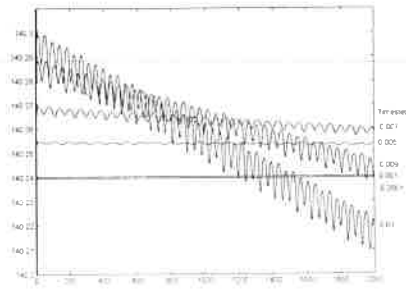
Figure 3. Energy Time History

Figure 4. Energy Sensitivity

B. Translational and Rotational Forced

This case directly specified the translational forces inside the CFD solver. The objective is to verify the constant force displacement motion. The non-dimensional forces in each coordinate direction are: $F_x = 0.25$, $F_y = 0.5$, $F_z = 1.0$. Since the forces are uncoupled when viewed in each orthogonal coordinate system, the displacement motion's form in each coordinate direction is:

$$d_i(t) = \frac{1}{2}\frac{F_i}{M}t^2$$

The CFD solver was hard-coded to represent the above forces. Figure 5 shows the translational displacements from 0 to 5 seconds with a mass of $1/500$.[b] The solution for z(t) is:

$$z(t) = 250\,t^2$$

At time 5, the error between theory and the solver is 1.5 out of 6250. The dynamics output matches theory.

Likewise, the rotational degree of freedom is tested. Figure 6 shows the dynamic solver Euler angles versus theory for an accelerating roll. The roll Euler angle, Φ, maps between $\pm\pi$ regardless of the total rolled angle. Thus, the solution for Φ is:

$$\Phi(t) = 2.5\,t^2 - 2n\pi$$

The error at time 5 is 0.04 out of 62.5 total radians of rotation. Again, the dynamic solver matches theory.
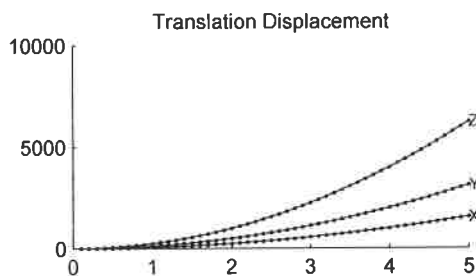
Figure 5. Translational Forced Displacement
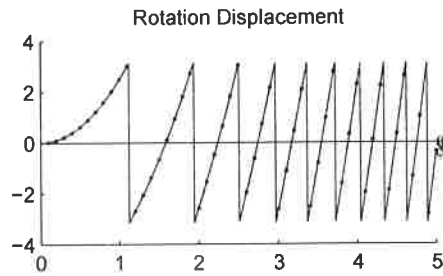
Figure 6. Rotational Forced Displacement

C. Simple Pressure Field Motion

The objective of this section is to verify that the CFD solver's pressure integration is input correctly into the rigid body simulation. This case will test the CFD pressure to rigid body coupling. A simple pressure field was specified:

$$p^*(x, y, z, t) = \begin{cases} 1 & \text{if } z > \epsilon \\ -1 & \text{if } z < \epsilon \\ 0 & \text{otherwise} \end{cases}$$

---

[b]The 1/500 mass ratio occurs because the CFD forces are scaled by dynamic pressure.

American Institute of Aeronautics and Astronautics Paper 2005-0230

Since the trailing edge does not *exactly* lie at $z = 0$, an ϵ parameter is used to prevent pressure wrap-over on the trailing edge node.

The pressure field is shown in Figure 7. Conceptually, the pressure above the zero waterline is greater than below. For reference, the dimensional pressure is 1000 psf. With a rotation point at the leading edge, the theoretical pitch moment is 20 ft-lb or 0.04 (non-dimensional). The time and moment response is given in Figure 8. The integrated CFD moment gives 0.0392; the error occurs in the finite length of the trailing edge element. This test concludes the verification process.

Figure 7. Specified Pressure Field
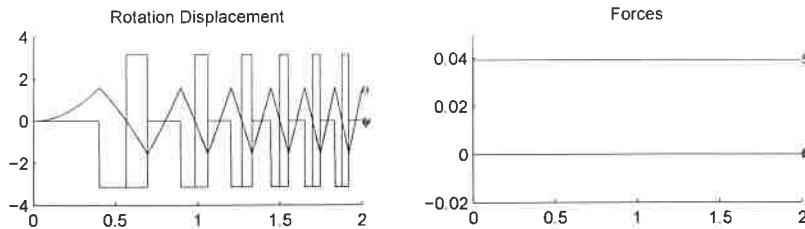
Figure 8. Specified Pressure Motion and Forces

VIII.   Validation

The objective of this section is to validate the dynamics solver with quasi-steady aerodynamics solutions. Both the translational and rotational frames are tested.

A.   Translational Rate Damping

This testcase tests the z-axis translational motion with airfoil rate damping. The concept (Fig. 9) is to allow an airfoil to reach a steady state upward velocity —via the airfoil's lift— when starting from an initial angle of attack, α_0. Intuition indicates that the final upward translational velocity will be such to provide an effective angle of attack of zero.
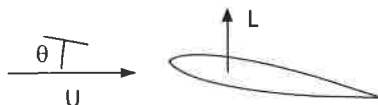
Figure 9.   Translation Rate: Geometry

Assuming quasi steady aerodynamics, the lift is a linear function of the instantaneous angle of attack. For this problem, the effective angle of attack comes from an initial angle of attack, α_0, and a plunging velocity to freestream ratio, $\dot{x}(t)/V$. Thus, the governing equation is:

$$m\ddot{x}(t) = qC_{L_\alpha}S\left(-\arctan\frac{\dot{x}(t)}{V} + \alpha_0\right)$$

When assuming small angles, $\arctan\frac{x}{V}$ is approximately $\frac{x}{V}$. A solution to the above differential equation is:

$$x(t) = \alpha_0 Vt - \frac{\alpha_0 V^2 m}{qC_{L_\alpha}S} + \frac{\alpha_0 V^2 m}{qC_{L_\alpha}S}\exp\left(-\frac{qC_{L_\alpha}St}{mV}\right)$$

The solver (dots) and theory (lines) predictions are shown in Figure 10. As expected, a steady state velocity is reached. The dynamics solver matches theory, which appears to suggest that the dynamic solver's translational displacement and velocity are properly passed to the CFD solver's boundary conditions.
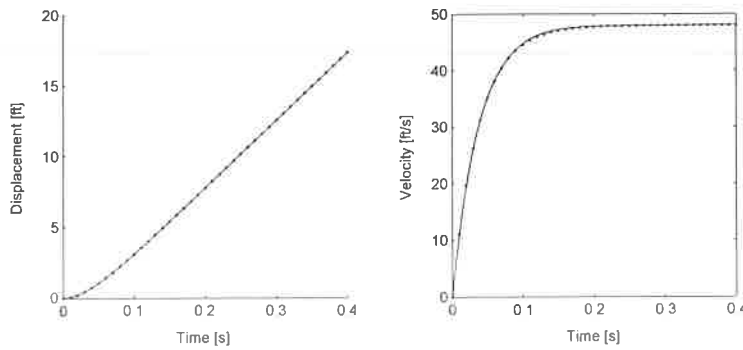
American Institute of Aeronautics and Astronautics Paper 2005-0230

Figure 10. Translation Rate: Lift

B. Rotational Rate Damping

This testcases's objective is to validate a rotational degree of freedom. An airfoil *slit* is rotated axially about an inboard axis. A rotation rate, ω, creates an effective angle of attack at the airfoil of $\alpha = \arctan(\omega L/U)$. Figure 11 shows the geometry. The governing equation of motion when assuming quasi-steady aerodynamics is:

$$\ddot{\phi}(t) = \frac{-LqcSC_{L_\alpha}}{I} \arctan \frac{\dot{\phi}L}{U}$$

The case has an initial rotation velocity of 90 degrees per second, a velocity of 500, and a axis offset of 16. The rotational rate damping response is shown in Figure 12 for theory (lines) and the dynamic solver output (dots). The rotational degree of freedom appears to work correctly.
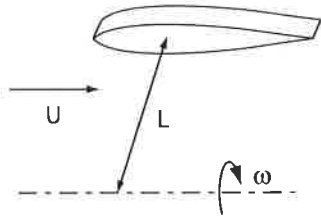
Figure 11. Rotating Rate Damping Geometry
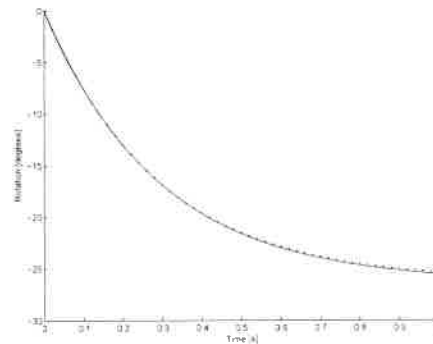
Figure 12. Rotating Rate Damping Response

IX. Flight Dynamics

Flight dynamics concerns the interaction between aerodynamics and a rigid body with respect to aircraft motions. An aircraft undergoing common maneuvers and a rotating wedge are presented.

A. Simplified General Aviation

A Navion general aviation aircraft was approximated with simplified geometry. The aircraft consists of a wing, horizontal, and vertical. Figure 13 shows the geometry. Figure 14 shows the surface Mach distribution at $\alpha = 0$ and $\beta = 0$ for 174 ft/s at SSL. Mass and sizing information comes from Nelson.[4]
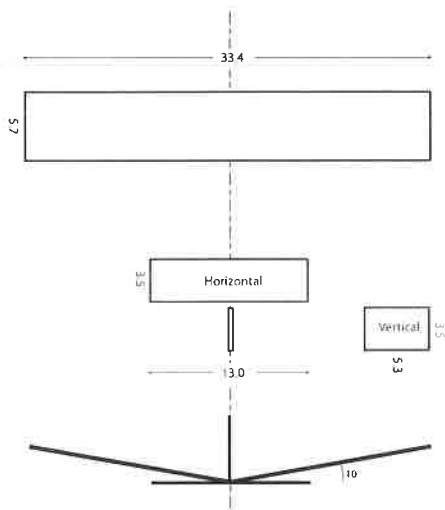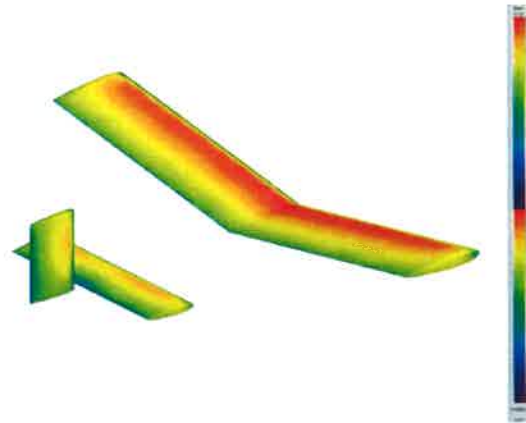
Figure 13. Navion Geometry

Figure 14. Navion 174 ft/s Mach Distribution

1. Rudder/Dihedral Response

The dihedral roll moment effect can be created with a rudder input. This case considers the stick-fixed free response for an initial left rudder input of 20 degrees. Again, the Navion's states are: V=174 ft/s, stick-fixed, and zero bank, pitch, and yaw angle. For easier visualization, gravity is removed. Intuition suggests that the *near* constant yaw angle will cause a roll moment, which causes a roll rate.

Figure 15 shows the translational and rotational motions. The deflected rudder rolls the aircraft in the expected barrel-roll maneuver in about 8 seconds. Figure 16 shows a visual representation of the aircraft's trajectory. The yaw angle is visible.
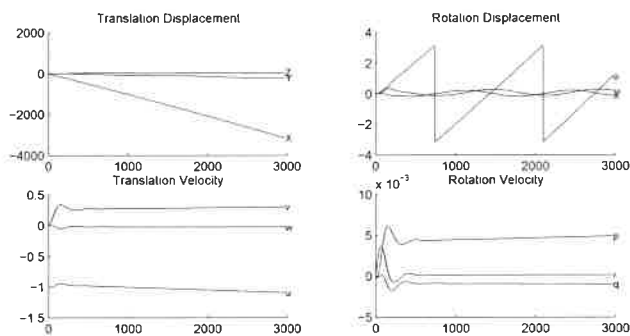
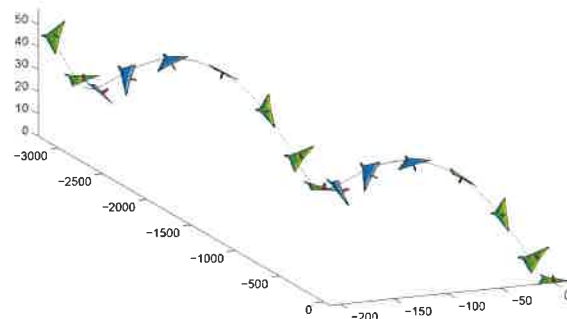**Figure 15. Navion Rudder/Dihedral Response Time History**

Figure 16. Navion Rudder Response Trajectory

2. Loop

This case's objective is to loop the Navion with a constant elevator deflection. To ensure sufficient energy to complete the maneuver, the aircraft begins inverted at the top of the loop. Initial conditions are 174 ft/s and a 20 degree elevator deflection.

The trajectory for the first case with the CG at 30% MAC (Fig. 17) shows a successful loop with the expected tightening at the top and an overall loss of altitude. Aircraft attitudes during the loop are visually consistent with reality.

Case 2 considers the same Navion aircraft and initial conditions but with the CG at a vastly tail-heavy and statically unstable 88% MAC. Figure 18 shows the trajectory with a stall/fall-out coming through the loop's bottom. Visually, the aircraft is pitch unstable.
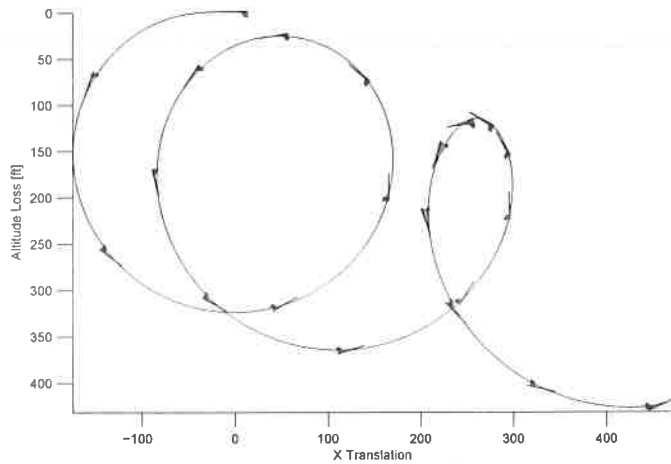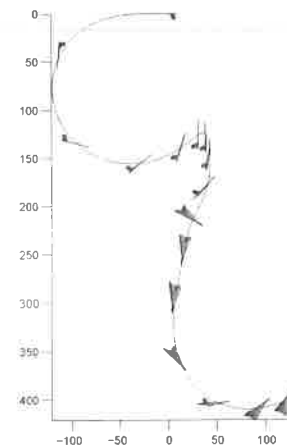
Figure 17. Navion Loop

Figure 18. Navion Loop with Fall Out

3. Spin

Spinning aircraft exhibit non-linear behavior. This spin case considers the Navion with 20 degrees up-elevator and 20 degrees left-rudder. Initial conditions are a negative vertical velocity with an initial yaw rate. Spin entry is not considered. Also, the inviscid Euler solution is likely to attenuate the separation for this viscous dominated *stalled* airfoil flow. Figure 19 shows the translational and rotational motions. From the low, non-increasing forward velocity and the harmonic rotational motion, the maneuver appears to be a spin and not a spiral motion. Altitude loss is approximately 500 feet per turn —interestingly consistent with reality when considering the inviscid Euler solution. The spin trajectory (Fig. 20) also appears consistent with an actual spin's behavior.
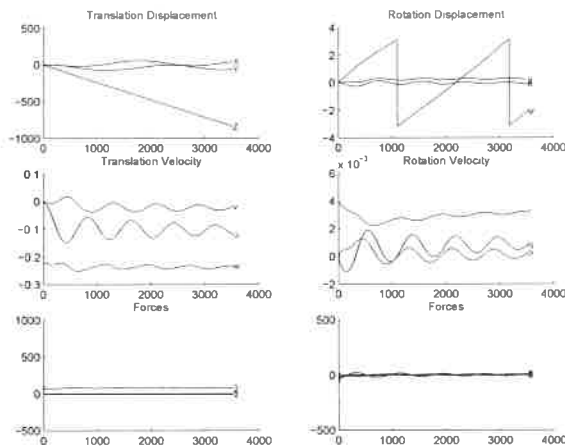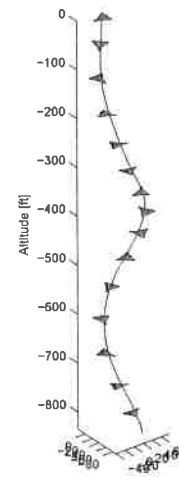

Figure 19. Navion Spin Motion

Figure 20. Navion Spin Trajectory

B. Wedge Drop

This case simulates a 10% thick wedge, free to translate and rotate, being dropped in air. The concept is to release the wedge *flat* from rest. A pair of vortices form off the sharp wedge edges, which eventually degenerate into a vortex street with an asymmetrical pressure distribution. The translational and rotational motions are shown in Figure 21. The wedge's CG trajectory is shown in Figure 22 with tick marks at each 1/2 second.
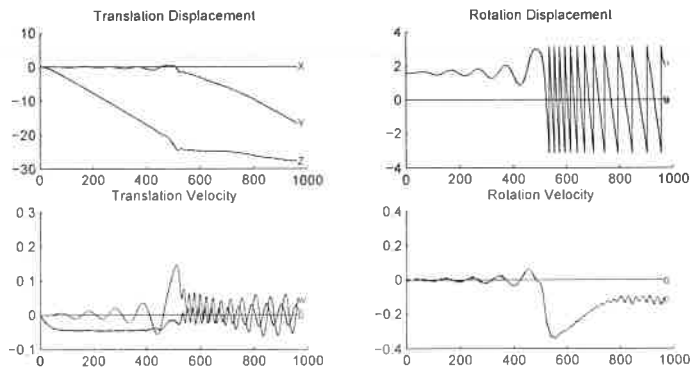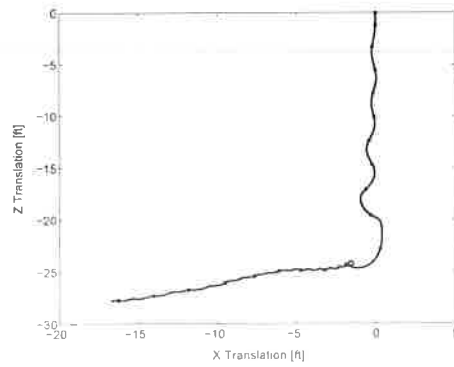
Figure 21. Wedge Time History

Figure 22. Wedge Trajectory

Initially, alternating vorticies appear to form causing a tumbling leaf motion. Interestingly, the wedge transitions to a *lift generating* Magnus motion with an apparent L/D of near 4. This experiment qualitatively matches the tumbling behavior of thin, light strips.

X. Stability Derivatives

Time-marched rigid body dynamics solutions as described above are expensive, general non-linear solutions. Stability derivatives are a traditional approach to simplifying aerodynamics by decomposing the dominant aerodynamics to the forces and moments caused by specific boundary condition. The rigid body dynamics solver's development allows for simplified boundary condition specification for simplified stability derivative extraction.

An advantage for stability derivative extraction, non-inertial CFD frames allows for direct, uncoupled boundary condition specification. This section replicates Babcock's method[12] with a direct boundary condition specification scheme.

A. Finned Missile

This case determines stability derivatives for the finned missile commonly known as the Finner using the rigid body dynamics solver and euler3d CFD solver. The missile has a standardized and well tested geometry[13–15] (Fig. 23). The overall geometry consists of a cone connected to a cylinder with fins. Figure 24 shows the corresponding finite-element CFD surface grid. Computational results are compared with experimental stability derivatives.[13, 14]
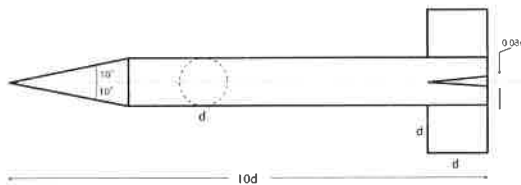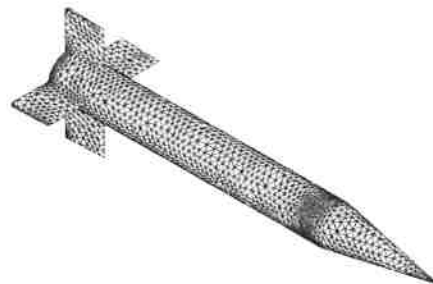

Figure 23. Finned Missile Geometry

Figure 24. Finned Missile CFD Grid

1. C_{M_α} Pitch Moment Angle Derivative

This case determines the pitch moment due to angle of attack, C_{M_α}. Pitch moment for the finned missile is non-dimensionalized by cross-sectional area and diameter: $M = q\frac{\pi}{4}d^3 C_M$. At a free-stream Mach of 1.6, C_{M_α} per radian is estimated as -41.8, which compares with -40 to -43 for experimental results.[13, 14]

2. C_{L_p} Roll Moment Rate Derivative

This case determines the roll moment due to roll rate, C_{L_p}. Roll Moment is dimensionalized by: $L = q\frac{\pi}{4}d^3 C_L$. The Mach 1.6 roll moment derivative C_{L_p} is estimated as -32.5, which compares with the experimental results of -30 in NAVORD[15] to -27 in DREV.[13,14] At Mach 2.4, the roll moment derivative is -17.7. The experimental derivative in DREV[13] is -18.

3. $C_{N_{\dot{w}}}$ Plunge Force Apparent Mass Derivative

The rigid body dynamics solver allows for unusual boundary condition specifications. This case determines the rarely reported plunge force apparent mass $C'_{N_{\dot{w}}}$. The derivative is expected to result from physics similar to the apparent mass terms in the Theodorsen problem. Plunge force is non-dimensionalized by: $N = q\frac{\pi}{4}d^3 C_N$. Also, the $C_{N_{\dot{w}}}$ derivative —for this paper— is defined as:

$$C_{N_{\dot{w}}} = \frac{\partial C_N}{\partial \left(\frac{\dot{w}d}{V^2}\right)}$$

The Mach 1.6 derivative $C_{N_{\dot{w}}}$ is estimated to be -900. No experimental data exists for this derivative.

B. Transonic F-18

F-18B stability derivatives are estimated in this section. The F-18's finite element grid has 2.18 million elements and was solved with the inviscid euler3d CFD code. Derivatives were determined for Mach 0.90 and Mach 1.30 and compared with flight test data from Moes.[16]

The resulting stability derivatives compare favorably with the experimentally determined flight test derivatives. However, the Mach 1.30 results generally show better agreement. Also, the experimental yaw axis derivatives appear relaxed because the flight test F18 has an extended canopy (two seat), while the CFD model is for the single seat F18. Only a subset —one angle and one rate— of the estimated derivatives are reported here.

Figure 25 shows the flight test data for the normal force derivative C_{N_α} from Moes with the CFD determined derivatives overlaid as dots. Figure 26 shows a comparison for pitch rate moment derivative C_{m_q}.
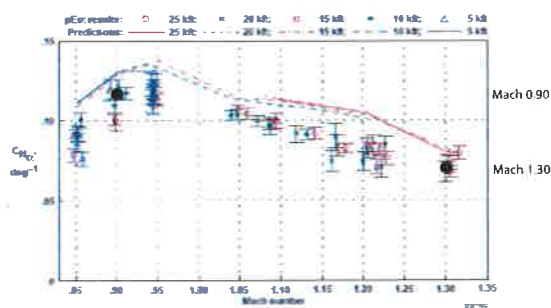

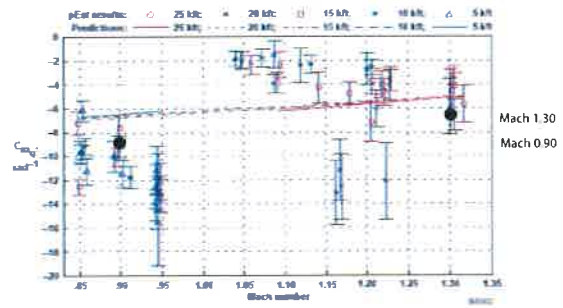Figure 25. F18B SRA C_{N_α}: Normal Force Derivative

Figure 26. F18B SRA C_{m_q}: Pitch Rate Moment Derivative

This stability derivative test-case shows the applicability of rigid body dynamics to actual aircraft stability and control extraction without solving the time-marched, coupled, rigid body dynamics differential equations.

XI.   Conclusions

This paper coupled a non-inertial aerodynamics CFD solver and rigid body dynamics solver. The CFD and rigid body governing equations are reviewed. This paper showed non-linear flight dynamics and stability derivative extraction.

A rigid body dynamics solver was successfully implemented. The quaternion orientation scheme appears preferable to Euler angles except for human visualization. The developed rigid body solver appears robust and accurate. Non-linear flight dynamics were simulated and appear qualitatively correct.

Overall, a non-inertial CFD formulation is shown to have significant advantages for rigid body dynamics and stability derivative extraction. A non-inertial formulation allows for a single, non-moving grid, while allowing direct motion specification. The current CFD solver used the inviscid Euler equations, which limited the solution quality in particular rigid body motions. Interesting rigid body dynamics appear correlated with viscous aerodynamics.

Stability derivative extraction as proposed by Babcock was presented. The rigid body solver's boundary condition specifications were coded for simplified use of a stability derivative extraction method. Extracted stability derivatives appeared consistent with experimental derivatives.

XII.   Acknowledgments

References

[1]Gupta, K. K., "Development of a Finite Element Aeroelastic Analysis Capability," *Journal of Aircraft*, Vol. 33, No. 5, September–October 1996, pp. 995–1002.

[2]Gupta, K. K., Bach, C., Doyle, T., and Hahn, E., "CFD-based Aeroservoelastic Analysis with Hyper-X Applications," AIAA Paper 2004-0884, 42nd AIAA Aerospace Sciences Meeting and Exhibit, Reno, NV, January 2004.

[3]Cowan, T. J., *Finite Element CFD Analysis of Super-Maneuvering and Spinning Structures*, Ph.D. thesis, Oklahoma State University, Stillwater, OK, August 2003.

[4]Nelson, R. C., *Flight Stability and Automatic Control*, McGraw-Hill, Boston, MA, 2nd ed., 1998.

[5]Phillips, W. F., Hailey, C. E., and Gebert, G. A., "Review of Attitude Representations Used for Aircraft Kinematics," *Journal of Aircraft*, Vol. 38, No. 4, July–August 2001, pp. 718–737.

[6]Stevens, B. L. and Lewis, F. L., *Aircraft Control and Simulation*, Wiley, New York, NY, 1st ed., 1992.

[7]Kato, O., "Some Basic Considerations on Angles Describing Airplane Flight Maneuvers," *Journal of Guidance, Control, and Dynamics*, Vol. 17, No. 2, March-April 1994, pp. 378–384.

[8]Tomaro, R. F., Witzeman, F. C., and Strang, W. Z., "Simulation of Store Separation for the F/A–18C Using Cobalt$_{60}$," *Journal of Aircraft*, Vol. 37, No. 3, May-June 2000, pp. 361–367.

[9]Cenko, A., "Experience in the use of computational aerodynamics to predict store release characteristics," *Progress in Aerospace Sciences*, Vol. 37, No. 5, July 2001, pp. 477–495.

[10]Lijewski, L. and Suhs, N., "Time-Accurate Computational Fluid Dynamics Approach to Transonic Store-Separation Trajectory Prediction," *Journal of Aircraft*, Vol. 31, No. 4, 1994, pp. 886–891.

[11]Rizk, M. and Lee, J. M., "Beggar Code Implementation of the (6+)DOF Capability for Stores with Moving Components," AIAA Paper 2004-1251, 42nd AIAA Aerospace Sciences Meeting and Exhibit, Reno, NV, January 2004.

[12]Babcock, D. and Arena, A., "Estimating Aircraft Stability Derivatives Through Finite Element Analysis," AIAA Paper 2004-5174, AIAA Atmospheric Flight Mechanics Conference and Exhibit, Providence, RI, August 2004.

[13]Dupuis, A. D. and Hathaway, W., "Aeroballistic Range Tests of a Basic Finner Reference Projectile at Supersonic Velocities," DREV-TM-9703, August 1997.

[14]Oktay, E. and Akay, H. U., "CFD Predictions of Dynamic Derivatives for Missiles," AIAA Paper 2002-0276, 40th AIAA Aerospace Sciences Meeting and Exhibit, Reno, NV, January 2002.

[15]Regan, F. J., "Roll Damping Moment Measurements for the Basic Finner at Subsonic and Supersonic Speeds," NAVORD Report 6652, June 1964.

[16]Moes, T. R., Noffz, G. K., and Iliff, K. W., "Results From F-18B Stability and Control Parameter Estimation Flight Tests at High Dynamic Pressures," NASA–TP–2000-209033, November 2000.